atmosphere

Article

Drivers of Spatial and Temporal Variability in Oil and Gas Emissions: Temporally Resolved Inventories for the Permian Basin Across Multiple Spatial Scales

Qining Chen, Sewar Jennifer Almasalha, Shannon Stokes, Lea Hildebrandt Ruiz and David T. Allen *

Center for Energy and Environmental Systems Analysis, University of Texas at Austin, 3925 West Braker Lane, Austin, TX 78759, USA; qnchen@utexas.edu (Q.C.); ssa2879@my.utexas.edu (S.J.A.); stokessn@austin.utexas.edu (S.S.); lhr@che.utexas.edu (L.H.R.)

* Correspondence: allen@che.utexas.edu

Abstract

Emission inventories at fine spatial and temporal scales were developed for light alkanes, volatile organic compounds (VOCs), and nitrogen oxides (NO_x) from upstream and midstream oil and gas operations in the Permian Basin oil and gas production region for 2022–2024. The inventories were spatially aggregated at basin, county, and 12 km by 12 km grid cell levels, and temporally resolved at hourly resolution, with underlying methods capable of generating inventories at other spatial and temporal scales. Spatial and temporal variability in emissions in the Permian were compared at various spatial scales with inventories for the Marcellus oil and gas production region, developed using the same methods. Emission sources that drive spatial and temporal variability differ by regional production characteristics, the level of spatial aggregation, and emitted species. Temporal variability in emissions decreases as the scale of spatial aggregation increases. Among counties with at least 10 active producing wells, maximum-to-annual-average hourly emission rate ratios reached 2.5 for methane, 2.8 for VOCs, and 2.3 for NO_x. At the 12 km by 12 km grid cell level, the corresponding maximum ratios were 33.7, 26.5, and 13.9. These ratios illustrate the magnitude of short-term emission variability and the extent to which peak hourly emissions can exceed annual average estimates, with potential implications for episodic air-quality impact assessment. Compared with the gas-dominated Marcellus Basin, the oil-dominated Permian Basin shows lower temporal variability in hydrocarbon emissions due to fewer episodic gas production related sources (e.g., liquid unloadings) and a greater contribution from near-continuous oil production related sources (e.g., associated gas venting and tank flash). In contrast, NO_x emissions exhibit higher temporal variability in the Permian due to more frequent preproduction activities associated with new well development. The spatially and temporally resolved emission inventories by source category and chemical species can be further combined with chemical transport modeling and air quality modeling to support assessment of regional air quality events, such as localized and episodic ozone formation.

Keywords: emission inventory; spatial variability; temporal variability; methane emissions; volatile organic compounds (VOCs); nitrogen oxides (NO_x); ozone formation; oil and gas production; Permian

Check for updates

Academic Editor: Qiang Song

Received: 31 July 2026
Revised: 3 September 2026
Accepted: 4 September 2026
Published: 5 September 2026

1. Introduction

The Permian Basin, located in western Texas and southeastern New Mexico, is one of the largest oil and gas producing regions in the United States. In 2024, production in the basin averaged 6.3 million barrels of oil per day and 25.4 billion standard cubic feet of natural gas per day, accounting for nearly half of total U.S. crude oil production and 22% of U.S. natural gas production. While oil and gas production in most other U.S. oil and gas producing regions, such as the Eagle Ford, Bakken, and Appalachia, remained relatively flat from 2023 to 2024, production in the Permian Basin continued to grow. Oil and natural gas production increased by 0.37 million barrels per day and 2.7 billion standard cubic feet per day, respectively, accounting for nearly all of the growth in U.S. oil and gas production. The increased production was driven by continued development of new wells. In 2024, the Permian Basin had more than 300 active drilling rigs, accounting for over half of the active rigs operating in the United States [1,2]. The rapidly growing oil and gas production in the Permian is accompanied by increased emissions of greenhouse gases, such as carbon dioxide and methane, and increased emissions of volatile organic compounds (VOCs) and nitrogen oxides (NO_x), which are precursors for atmospheric ozone formation.

The frequent development of new wells in the Permian Basin underscores the need for spatially and temporally resolved emission inventories, especially for emissions of ozone precursors. Activities associated with new well development, such as drilling, hydraulic fracturing, and well completion that occur over short periods of time and at locations that change frequently, may introduce significant temporal and spatial variability in oil and gas emissions that can lead to localized formation of ozone [3]. In addition, oil and gas emissions exhibit substantial spatial and temporal variability. Spatial and temporal variability in emissions can be contributed not only by large unintended emission events, such as those from liquid storage tanks and equipment leaks [4–6], but also by intermittent, routine operations, such as extensive venting and flaring [7]. For example, intermittent methane venting from manual liquid unloadings at a relatively small fraction of well pads produced an approximately twofold temporal variation in the basin-scale methane emissions from dry gas production region in the U.S. [8].

Because ozone is regulated in the United States based on the highest observed concentrations of ozone, emission events that lead to rapid formation and accumulation of ozone can impact whether a region attains National Ambient Air Quality Standards. Inventories that rely on annual averaged activity and emission data or developed at coarse spatial and temporal resolution may not fully capture the variability and magnitude of emissions associated with ongoing development in the basin and may not accurately predict localized ozone formation events. For example, the U.S. Greenhouse Gas Inventory (GHGI) [9] provides annual national-scale estimates of greenhouse gas emissions, while the Greenhouse Gas Reporting Program (GHGRP) [10] reports annual emissions from facilities with emissions above certain thresholds. The National Emissions Inventory (NEI) [11], released every three years, includes facility-level emissions for point sources and county-level estimates for many nonpoint sources such as individual well sites. In Texas, the Texas Commission on Environmental Quality (TCEQ) Point Source Emissions Inventory [12] reports annual emissions from facilities that meet state reporting requirements. The annual reporting and spatial aggregation of these commonly used national and state emission inventories can limit their ability to capture fine-scale spatial and temporal variability associated with rapidly changing oil and gas activities. Inventories developed from recent studies based on multi-scale measurements have improved the spatial resolution but remain limited in their ability to represent short-term temporal variability. For example, Zhang et al. [7] developed a methane inventory for the Permian Basin at approximately 10 km grid resolution, representing annual emissions in 2018, and derived monthly methane emissions at ap-

https://doi.org/10.3390/atmos17090870

proximately 30 km grid resolution from May 2018 to March 2019 using satellite inversions. Omara et al. [13] developed a methane inventory for the Permian Basin at approximately 1 km grid resolution, representing annual emissions for 2021. Methods for developing basin-wide, spatially and temporally resolved inventories have been reported in the Marcellus oil and gas production region [14]. Inventories for methane, ethane, VOCs and NO_x were developed at one-hour resolution for the year 2023 at the county level for the entire basin with >200,000 oil and gas production sites. Emissions were simulated using county-level “aggregated wells”, where each “aggregated well” represented the summed production volumes and equipment counts from wells with the same production type (e.g., dry gas, wet gas, or oil) within the county. These county-average well types could then be spatially allocated based on the locations of the wells and other facilities.

This work improves methods for developing large-scale, spatially and temporally resolved emission inventories across oil and gas production basins by performing emission estimation at the finest practical resolution for each source category, rather than utilizing county level average well characteristics. Emissions from sources with more complex spatial and temporal variability, such as from pre-production activities and liquid unloadings, are estimated at the individual well level, while other emissions are estimated at the grid cell or county level using spatially resolved activity data and emission factors derived from representative distributions of emissions. This level of detail is required in regions like the Permian Basin that have been in operation for much longer periods than regions like the Marcellus. In the Permian, wells with very different ages and equipment configurations are located in close geographical proximity. Consequently, county average configurations will not represent equipment configurations accurately. Emission inventories of light alkanes (methane, ethane, propane, butanes), VOCs, and NO_x in the Permian Basin for 2022 through 2024, from a total of ~170,000 well sites, were developed at the basin, county, and 12 km by 12 km grid cell levels, and temporally resolved at hourly resolution, with underlying methods capable of generating inventories at finer spatial scales. As a region dominated by oil production and with both older production operations and frequent new well development activities, the temporal and spatial distributions of emissions in the Permian Basin differ from those in newer gas production dominated regions, like the Marcellus. To demonstrate this contrast, temporal and spatial variability of predicted emissions in the Permian were compared to those in the Marcellus oil and gas production region.

This work provides a framework for developing large-scale, high-resolution inventories of oil and gas emissions, characterizing the distribution and variability of emissions, and identifying sources of spatial and temporal variability across different production scenarios, emission species, and spatial scales of emissions aggregation. The resulting inventory can be integrated with chemical transport modeling and air quality and health impact analyses to identify potential hotspots of elevated air pollution. This framework can support assessment of the broader air-quality impacts of oil and gas development, including the identification of spatial and temporal patterns in ozone precursor emissions and their potential contributions to regional ozone formation.

2. Methodology

2.1. Study Domain and Emission Sources

The Permian Basin study domain consists of 62 counties in Texas and 4 counties in New Mexico, 60 of which had at least 1 active producing well during 2022–2024; 55 of those had at least 10. County boundaries and locations of active producing well sites, midstream sites, and flare sites are shown in Figure 1, representing production in the year 2023. The study domain was divided into 12 km by 12 km grids used in aggregating the emission inventories. Annual production, active producing well counts by production type, and the number of completions in the year 2023 and in other simulation years are summarized in Table 1 and in the Supporting Information (SI).

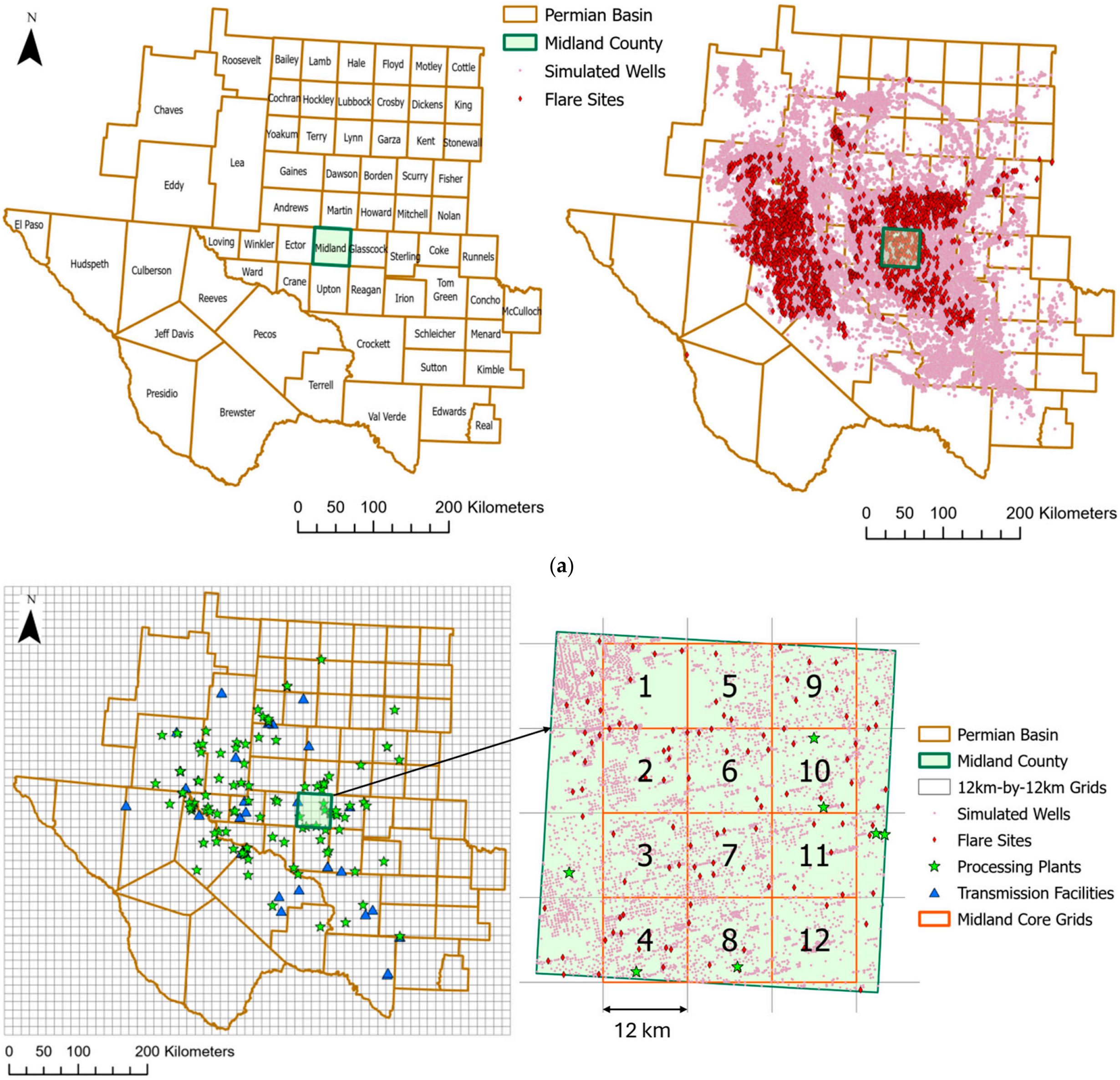

(**a**)

(**b**)

Figure 1. (**a**) County boundaries used for inventory aggregation (**left**) and locations of active producing well sites and flare sites within the study domain in 2023 (**right**); (**b**) locations of gas processing plants and transmission facilities overlaid with 12 km by 12 km grid cells and county boundaries (**left**), and a zoomed-in view of Midland County and the core grid cells (**right**).

Emissions from a total of ~170,000 wells within the Permian Basin, with active production in 2022, 2023, and 2024, were simulated. Of these wells, ~80% are oil wells with >40% of total wellhead energy production associated with liquids; ~13% are wet gas wells with 1–40% of wellhead energy production associated with liquids; the remainder are dry gas wells with <1% of wellhead energy production associated with liquids. On average, around 6700 wells were completed or re-completed at least once each year, about 90% of which were new wells brought into production. Among the three simulation years, 2023 had the highest number of new wells, with nearly 7000 completions [15].

Table 1. Annual production, active producing well counts by production type, and number of completions in the Permian Basin and in Midland County in 2023.

	Permian Basin	Midland County
Annual gas production (BCF)	8520	830
Annual oil production (million BBL)	2174	234
Annual water production (million BBL)	8384	597
Total active wells simulated	155,985	8549
Number of wells completed	6968	643
Number of completions	6995	642
Dry gas wells	12,227	0
Wet gas wells	19,796	378
Oil wells	123,962	8171

Inventories of methane, ethane, propane, butanes, volatile organic compounds (VOCs) and NO_x were developed for the years 2022–2024 at three spatial levels: the 12 km by 12 km grid cell level, the county level, and the basin level. Emission sources in the study domain include pre-production sources (including drilling engines, hydraulic fracturing pumps, and well completions), production sources (including artificial lift engines, associated gas venting, condensate and water tank flash, pneumatic controllers, chemical injection pumps, heaters, liquid unloadings, and leaks), as well as emissions from gathering compressor stations, gas processing plants, gas transmission facilities, and flare sites. Locations of well sites (for pre-production and production sources) were determined from public data [15]. Gathering and boosting sites were assumed to be evenly distributed, with nine sites per 12 km by 12 km grid cell. This corresponds to one site per 4 km by 4 km sub-grid, obtained by dividing each 12 km by 12 km grid cell into nine equal cells, which is consistent with the density of gathering and boosting sites observed in satellite imagery [16]. Gas processing plants and transmission facilities were obtained from the U.S. Environmental Protection Agency (EPA) Greenhouse Gas Reporting Program (GHGRP) [10] and manually verified using satellite imagery [17]. Flare locations were based on annual gas flaring estimates [18–21] with Visible Infrared Imaging Radiometer Suite (VIIRS) observations [22].

Midland County in Texas, located in the center of the Permian Basin, was selected as a case study region for detailed emissions modeling for 2023 and 2024. Annual production, active producing well counts by production type, and the number of completions in 2023 in Midland County are summarized in Table 1, with corresponding data for 2024 provided in the Supplementary Materials. Midland County is one of the most active producing areas in the basin. In 2023, 8549 wells were actively producing in the county, representing 5.5% of the total well count in the basin. Gas and oil production from Midland County accounted for about 10% of the total gas and oil production in the basin [15]. All well site sources in Midland County were simulated at the individual well level before being aggregated into grid cells, with additional grid- and county-level simulations generated for comparison to evaluate the effectiveness of simulations at aggregated spatial scales. The twelve core grid cells used to aggregate well-level simulations, with most of each grid cell lying within the county boundary, are shown in Figure 1. In other parts of the basin, most well site sources were represented only at the grid or county levels to reduce computational requirements, as described in later sections.

2.2. Emission Compositions

Source-specific hydrocarbon emission compositions were estimated using the Emission Composition Tool (ECT), a searchable thermodynamic database constructed with empirical data and thermodynamic models [23]. The ECT predicts composition profiles for well stream, produced gas, condensate tank flash, and water tank flash, by returning the closest matching record in the database. The match is based on a set of inputs including separator operational parameters (pressure and temperature), well production characteristics (API gravity of liquids produced and gas-to-oil ratio of the well), and produced gas compositions. Median values of separator pressure (200 psia) and temperature (80 °F) based on public data reports in the Permian Basin, and average API gravity (51.5°), gas-to-oil ratio (11,500 SCF/BBL), and produced gas compositions (methane: 72.9%, ethane: 13.8%, and propane: 6.83%, by molar fraction) based on public data available for Midland County and Andrews County in Texas, were used as input [16]. Predicted compositions of methane, ethane, propane, n-butane and iso-butane, and VOCs for each composition profile are summarized in Table 2. The sum of propane and butane emissions was used as a surrogate for VOC emissions from condensate tank flash. The predicted compositions represent typical conditions in the Permian Basin but do not capture potential spatial variability in hydrocarbon compositions across the basin. This may affect the magnitude of species-specific emission estimates in different regions. However, this limitation is not expected to substantially affect the spatial and temporal distribution of emissions.

Table 2. Hydrocarbon emission compositions applied in inventories.

Composition Profile	Methane	Ethane	Propane	n-Butane	iso-Butane	VOCs
Produced gas (molar fraction)	74.3%	14.8%	6.06%	1.68%	1.05%	9.76%
Well stream (molar fraction)	68.0%	14.0%	6.22%	2.18	1.25	16.96
Condensate tank flash (kg/bbl oil produced)	1.03	2.02	4.06	4.90	2.19	11.2 *
Water tank flash (kg/bbl water produced)	0.0359	0.0187	0.00895	0.00267	0.00461	0.0191

* Calculated as the total mass of propane and butanes in condensate tank flash.

The predicted hydrocarbon emission compositions were applied to emissions from all sources except drilling engines and hydraulic fracturing pumps, which use diesel fuel and therefore have different emission compositions than estimated using the ECT. For the sources with compositions estimated using the ECT, well stream compositions were applied to emissions from well completions and liquid unloadings; condensate tank flash and water tank flash compositions were applied to condensate and water tank flash; and produced gas compositions were applied to all the other sources except leaks. Leak compositions were assigned either produced gas or well stream compositions, depending on the leak location [24].

Emission compositions of drilling engines and hydraulic fracturing pumps were obtained from the EPA 2020 Nonpoint Oil and Gas Emission Estimation Tool (V1.3) (referred to as the EPA Nonpoint Oil and Gas Tool in the following text) [25], as described by Chen et al. [14]. Only methane, VOCs, and NO_x emissions were estimated for these sources, and other hydrocarbon emissions were assumed to be negligible.

NO_x emissions were estimated only for sources involving combustion. For well site combustion sources including drilling engines, hydraulic fracturing pumps, artificial lift engines, and heaters, NO_x emissions were estimated using the EPA Nonpoint Oil and

Gas Tool [25]. For gathering compressor stations, gas processing plants, gas transmission facilities, and flares, NO_x emissions were estimated by applying NO_x-to-methane ratios calculated from EPA AP-42 emission factors [26] to the portion of methane emissions attributed to combustion. Methods were described by Chen et al. [14].

2.3. Emission Estimation Methods

Hydrocarbon and NO_x emissions were estimated using publicly available models, including the Methane Emission Estimation Tool (MEET) [27], the EPA Nonpoint Oil and Gas Tool [25], the Inventory of U.S. Greenhouse Gas Emissions and Sinks (GHGI) [9], U.S. Greenhouse Gas Reporting Program (GHGRP) [10], Compilation of Air Pollutant Emissions Factors from Stationary Sources (AP-42) [26], and empirical models and datasets based on field measurements [28–32] and satellite observations [18,22]. Emissions were estimated from source categories including pre-production sources (including drilling engines, hydraulic fracturing pumps, and well completions), production sources (including artificial lift engines, associated gas venting, condensate and water tank flash, pneumatic controllers, chemical injection pumps, heaters, liquid unloadings, and leaks), gathering compressor stations, gas processing plants, gas transmission facilities, and flares.

In Midland County, pre-production and production sources that occur on well sites were simulated at the individual well level before being aggregated into the 12 km by 12 km grid cells. Detailed simulation methods per emission source were described in previous work [14,16]. For the basin wide simulation, these well site sources were simulated mostly at an aggregated spatial level, except for well completions and liquid unloadings which had more complex temporal characteristics. For these sources, simulations remained spatially assigned at the individual well level. The methods for simulating sources at an aggregated spatial level were described by Graves et al. [16]. Briefly, time series of aggregated activity data at the 12 km by 12 km grid level or county level were combined with averaged emission factors per source, to predict time series of emissions per source. Equipment counts per well for well-site equipment, including pneumatic controllers, chemical injection pumps, meters/piping, and heaters, as well as the fraction of wells with liquid unloading operations, used in emission estimates for 2022–2024 were taken consistently from the 2022 Inventory of U.S. Greenhouse Gas Emissions and Sinks (GHGI) [9], which was the most recent version available at the time the simulations were conducted. These activity data were expected to remain relatively stable over time. Other activity data, including locations of active producing wells, and gas, oil, and water production per well, were collected on a monthly basis, while pre-production and completion schedules were resolved on a daily basis.

Based on field observations, Chen et al. [14] assumed controls on tanks based on the existence of oil production on site. Both oil and water tanks were assumed to be present on well sites. Tanks on sites with oil production were assumed to be controlled at 95% efficiency, whereas tanks on sites with no oil production had no controls applied. Graves et al. [16] based the presence or absence of tank controls on regulatory requirements. Under federal regulation [33], control of methane emissions from tanks and other oil and gas sources has been required since 18 September 2015. Accordingly, a control efficiency of 95% was applied to wells with completion dates on and after 18 September 2015, while no controls were applied to wells completed earlier. In this work, the tank control strategy based on regulatory requirements was applied in the base case analyses, with an additional sensitivity scenario defining control strategy based on the volume of oil production provided in the Supplementary Materials.

For gathering compressor stations, gas processing plants, gas transmission facilities, and flares, emissions were estimated as site total emissions, as described in previous work [14,16]. Specifically, for gathering compressor stations, emission factors were developed as a function of site throughput are therefore highly sensitive to the throughput assigned to each compressor station [29]. However, site-specific throughput data for gathering compressor stations were not readily available. Nine compressor stations were assumed within each 12 km by 12 km grid cell. The total gas production within each grid cell was then evenly distributed among the nine compressor stations and used as the throughput for each site. The assumed uniform distribution of gathering compressor stations and the equal allocation of grid-level gas production among these stations within each 12 km by 12 km grid cell may affect site-level emission estimates and fail to capture spatial variability in emissions from gathering compressor stations within individual 12 km by 12 km grid cells. However, these assumptions are not expected to substantially affect emission estimates aggregated to the 12 km $\times$ 12 km grid-cell level, which is the finest spatial resolution used for inventory aggregation in this work.

Chen et al. [14] evaluated the effects of engine types (4-stroke lean-burn (4SLB) versus 4-stroke rich-burn (4SRB)) used in gathering compressor stations, gas processing plants, and gas transmission facilities on the temporal variability of NO_x emissions. Greater temporal variability in NO_x emissions was observed with 4SLB engines. 4SLB engines, which are more frequently observed in the field, were assumed in the base case scenario, with additional sensitivity runs using 4SRB engines provided in the Supplementary Materials.

3. Results and Discussion

3.1. Inventories at Various Spatial Scales

Figure 2 shows county-level distributions of active producing wells and annual average hourly emission rates of methane, VOCs, and NO_x in the Permian Basin in 2023. Counties with larger numbers of active wells generally show higher annual average hourly emission rates, particularly across southeastern New Mexico and western and central Texas. County-level hydrocarbon and NO_x emission rates span several orders of magnitude. Methane emission rates range from less than 10 to 15,695 kg/h, with a mean of 2155 kg/h and 25th, 50th and 75th percentiles of 112, 515, and 3006 kg/h, respectively. County-level VOC emission rates average 7028 kg/h, with corresponding percentiles of 230, 1555, and 11,158 kg/h and a maximum of 59,791 kg/h. County-level NO_x emission rates average 512 kg/h, with corresponding percentiles of 10, 61, and 368 kg/h and a maximum of 7644 kg/h. Average emission rates of methane, VOCs, and NO_x in Midland County are 8783, 28,247, and 1526 kg/h, representing emission rates within the top 5–10% among the 60 counties with active production in the basin.

Table 3 presents statistics of hydrocarbon and NO_x emissions for the basin and Midland County in the year 2023, with inventories simulated at the county level. Average hydrocarbon and NO_x emission rates in Midland County accounted for about 7% and 4%, respectively, of average hydrocarbon and NO_x emission rates in the basin. NO_x emissions exhibit greater temporal variability, with higher maximum to average emission rate ratios at both basin and county levels, compared to hydrocarbon emissions. Statistics of hourly emission rates for other simulation years are available in the Supplementary Materials. Hourly inventories for 2022, 2023 and 2024 by species by source aggregated in the Permian Basin and in Midland County are also provided in the Supplementary Materials. The comparison of Midland inventories simulated at the individual well level and then aggregated to the twelve core grids within the county (shown in Figure 1), versus those simulated directly at the 12 km resolution grid level is provided in the Supplementary Materials. The two inventories agree well in both emission magnitude and temporal variability, with differences in annual total emissions of less than 1% for both hydrocarbon and NO_x emissions when all sources are aggregated. Larger differences occur for some individual sources and are primarily due to differences in how active equipment and emission factors are assigned in the grid-level and well-level simulations, rather than the effect of spatial aggregation (see Supplementary Materials).

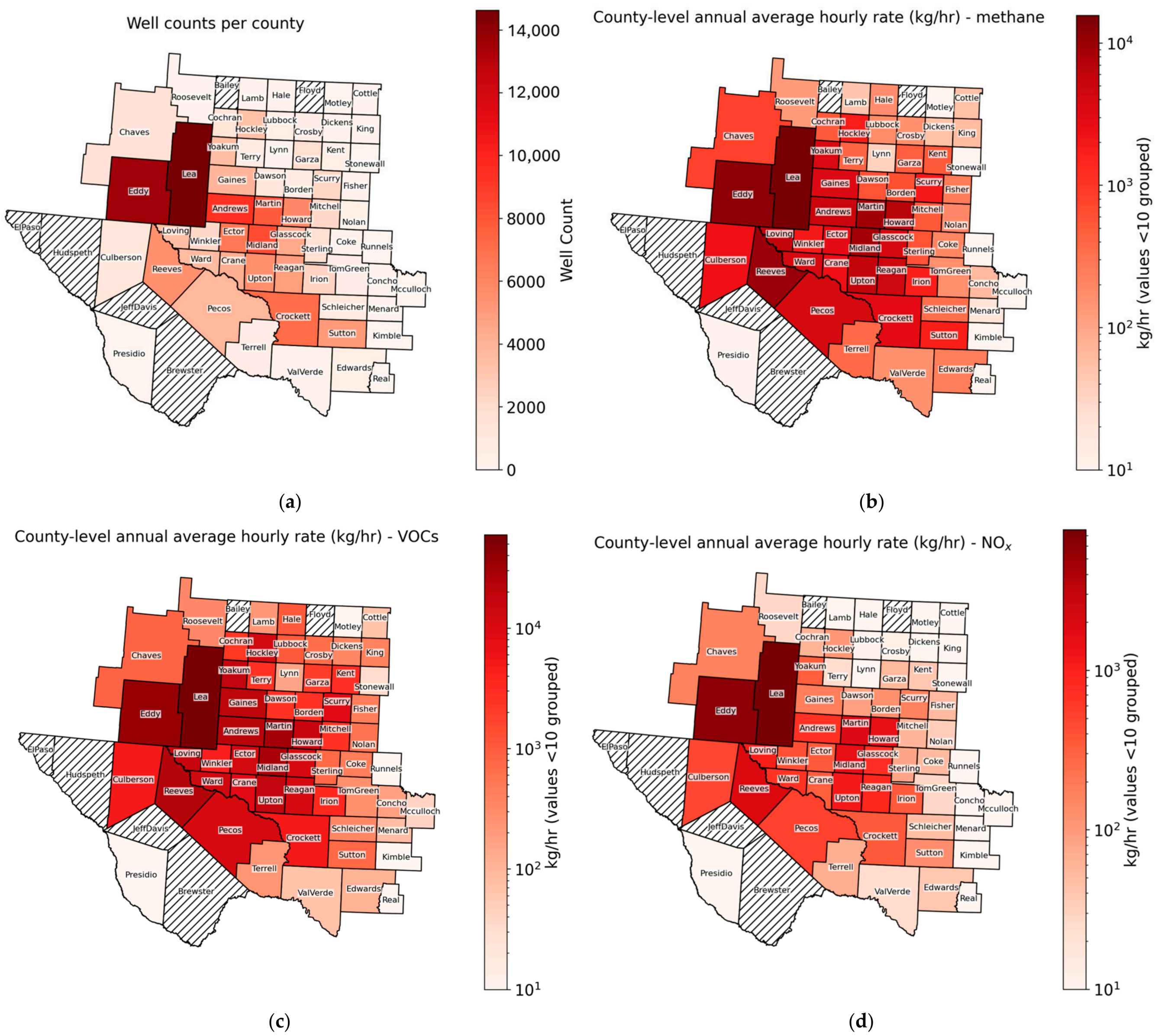

Figure 2. County-level distributions of (**a**) active well count and annual average hourly emission rates of (**b**) methane, (**c**) VOCs, and (**d**) NO_x across the Permian Basin in 2023. The six counties without active producing wells during 2022–2024 are filled with diagonal line patterns.

Table 4 presents the distribution of maximum to annual average hourly emission rate ratios among 805 12 km by 12 km grid cells and 55 counties with at least 10 active producing wells across the Permian Basin in 2023. An additional 207 grid cells and five counties with less than 10 active producing wells were excluded from statistical analyses to avoid bias associated with aggregating emissions from only a small number of sources. Maximum to average emission rate ratios decrease as the scale of spatial aggregation increases. At the county level, maximum hourly hydrocarbon emission rates could be about 2–3 times higher than the annual average hourly rate, whereas at the 12 km by 12 km grid cell level, maximum hourly hydrocarbon emission rates could be over 30 times higher than the annual average hourly rate. At the county level, hydrocarbon and NO_x emissions exhibit comparable temporal variability. At the grid level, however, NO_x emissions show higher temporal variability, due to the spatially and temporally clustered drilling and fracturing activities.

Table 3. Distributions of methane, ethane, propane, butanes, VOCs, and NO_x hourly emission rates for the basin and Midland County in 2023.

Species	Mean (Tonnes/h)	Median (Tonnes/h)	75th Percentile (Tonnes/h)	90th Percentile (Tonnes/h)	Max (Tonnes/h)	Max-to-Mean Ratio
			Basin			
Methane	129.3	129.2	130.2	131.2	134.9	1.04
Ethane	105.0	105.1	106.1	106.8	108.8	1.04
Propane	159.4	159.8	161.3	163.1	164.5	1.03
iso-Butane	79.71	80.01	80.81	81.72	82.20	1.03
n-Butane	174.1	174.8	176.6	178.6	179.5	1.03
VOCs	421.7	422.7	427.0	431.6	438.6	1.04
NO_x	30.76	30.72	31.81	32.82	34.48	1.12
			Midland County, TX			
Methane	8.783	8.737	8.957	9.104	9.774	1.11
Ethane	7.041	7.023	7.115	7.198	7.544	1.07
Propane	10.70	10.69	10.76	10.86	11.23	1.05
iso-Butane	5.326	5.324	5.357	5.386	5.547	1.04
n-Butane	11.68	11.68	11.75	11.80	12.14	1.04
VOCs	28.25	28.22	28.43	28.83	29.98	1.06
NO_x	1.526	1.525	1.795	1.929	2.314	1.52

Table 4. Distributions of maximum to annual average hourly emission rate ratios among 805 12 km by 12 km grid cells and 55 counties with at least 10 active producing wells across the Permian Basin in 2023.

Species	Mean	std	Min	25%	50%	75%	Max
			Distributions of ratios among 805 grids				
Methane	1.8	1.8	1.0	1.1	1.4	1.9	33.7
Ethane	1.5	1.1	1.0	1.1	1.3	1.5	18.6
Propane	1.4	0.7	1.0	1.1	1.2	1.4	11.0
iso-Butane	1.3	0.7	1.0	1.1	1.2	1.3	11.3
n-Butane	1.3	0.7	1.0	1.1	1.2	1.3	12.0
VOCs	1.7	1.7	1.0	1.2	1.3	1.5	26.5
NO_x	2.2	1.7	1.0	1.1	1.4	2.9	13.9
			Distributions of ratios among 55 counties				
Methane	1.3	0.3	1.0	1.1	1.2	1.4	2.5
Ethane	1.2	0.2	1.0	1.1	1.1	1.2	2.0
Propane	1.1	0.1	1.0	1.1	1.1	1.2	1.6
iso-Butane	1.1	0.1	1.0	1.1	1.1	1.2	1.7
n-Butane	1.1	0.1	1.0	1.1	1.1	1.2	1.7
VOCs	1.2	0.3	1.0	1.1	1.1	1.3	2.8
NO_x	1.4	0.3	1.0	1.2	1.4	1.5	2.3

Figure 3 shows county-level spatial distributions of maximum to annual average hourly emission rate ratios for VOCs and NO_x across the Permian Basin and grid-level distributions across the 12 core grid cells in Midland County. At the county level, the highest ratios occur in peripheral counties or counties with relatively few producing wells, where emissions from a small number of wells can lead to large temporal variability. Counties with at least 10 active producing wells show a relatively narrow distribution of ratios, as shown in Table 4. In Midland County, grid-level maximum to average emission rate ratios of VOCs vary within a narrow range of 1.2 to 1.6, while ratios of NO_x show greater spatial variability, ranging from 1.9 to 5.5.

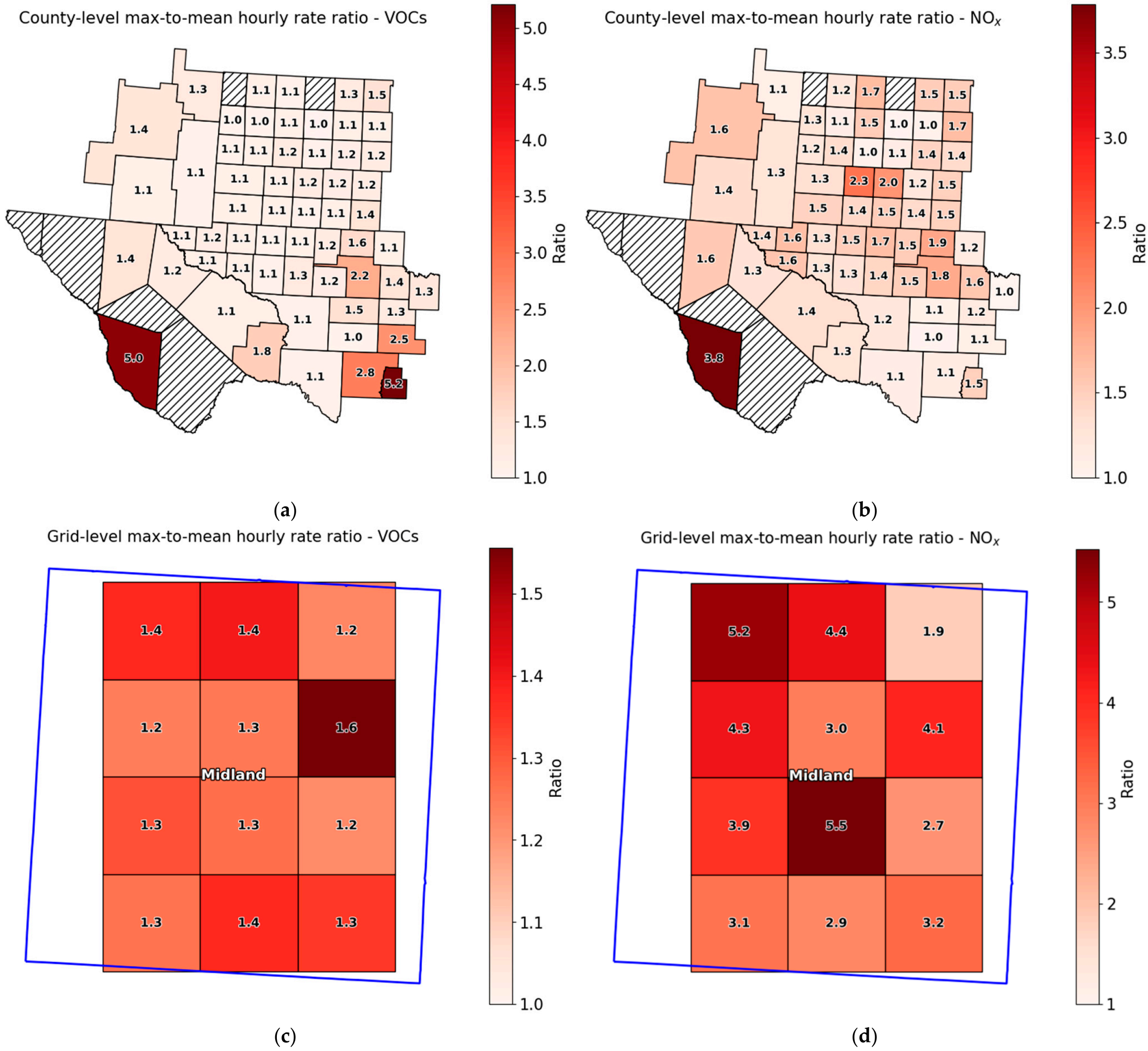

Figure 3. County-level distributions of maximum to annual average hourly emission rate ratios of (**a**) VOCs and (**b**) NO_x across the Permian Basin, and grid-level distributions for (**c**) VOCs and (**d**) NO_x across the 12 core grid cells in Midland County.

Hourly time series of methane, propane, and NO_x emissions in 2023, aggregated at the basin and Midland County level, are shown in Figures 4 and 5. Hourly time series of other species are available in the Supplementary Materials. Emission sources are grouped as preproduction sources (completion flowbacks, drilling engines, hydraulic fracturing pumps), tank flash (condensate and water tank flash), pneumatic devices (pneumatic controllers and chemical injection pumps), liquid unloading, wellsite—other routine emissions (associated gas venting, artificial lift engines, heaters, and leaks), flare, and midstream operations (gathering and boosting, processing plants, and transmission facilities).

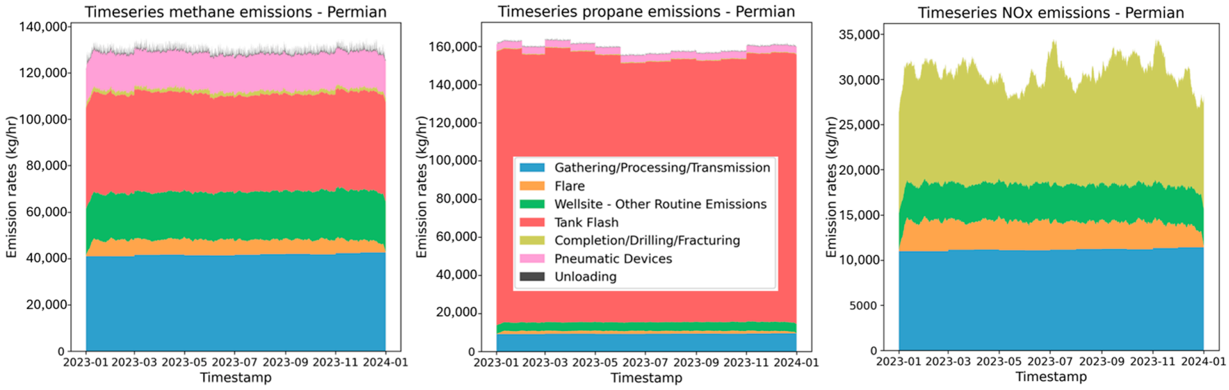

Figure 4. Hourly emission time series for methane (**left**), propane (**middle**), and NO_x (**right**) emissions in the Permian Basin in 2023.

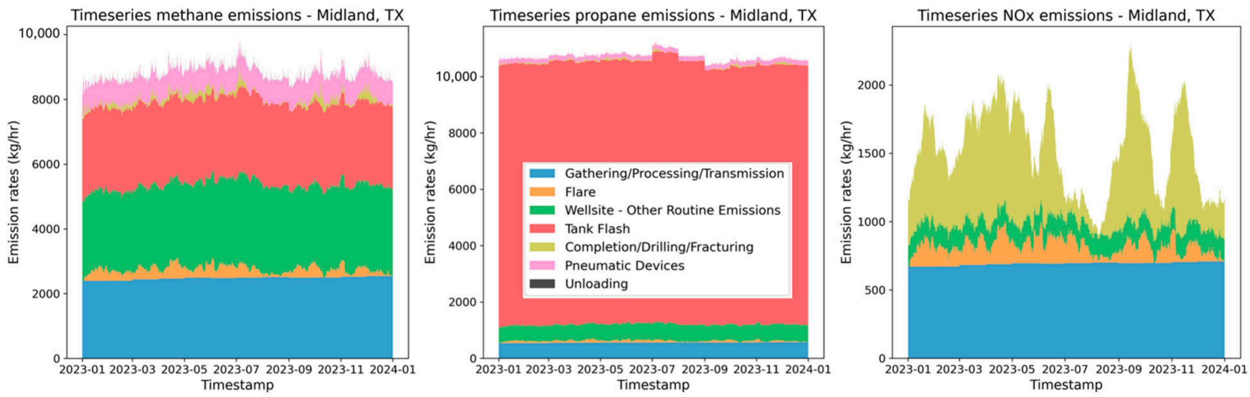

Figure 5. Hourly emission time series for methane (**left**), propane (**middle**), and NO_x (**right**) emissions in Midland County, Texas in 2023.

Basin and county-level methane emissions are dominated by tank flash, associated gas venting (categorized as wellsite—other routine emissions), and midstream operations. For higher molecular weight hydrocarbons, tank flash becomes the primary contributing source to county total emissions. Temporal variability in methane emissions is primarily driven by episodic flaring and liquid unloading events, whereas temporal variability in propane or heavier hydrocarbon emissions is dominated by monthly variations in tank flash emissions associated with variability in monthly water and condensate production rates. NO_x emissions show different temporal behaviors compared to hydrocarbon emissions and depend largely on the type of engines assumed for midstream operations [7]. With 4SLB engines in midstream operations that produce lower NO_x emissions on a consistent basis, temporal variability in basin- and county-level NO_x emissions is dominated by episodic preproduction activities, particularly drilling and fracturing. This variability would be largely reduced, though still significant, if midstream engines were 4SRB engines, which produce over 14 times more NO_x emissions compared to lean burn engines [26]. Additional sensitivity runs with 4SRB engines assumed in midstream operations are available in the Supplementary Materials.

Emission inventories were also aggregated into the 12 km by 12 km grid cells. At a finer spatial scale, temporal variability in both hydrocarbons and NO_x emissions increases.

Figure 6 shows hourly emissions time series of methane, propane, and NO_x emissions, in representative grid cells with highest maximum to average hourly emission rates ratios in Midland County in 2023. Newly developed wells have a larger influence on grid-level emissions compared to county- and basin-level emissions. At the grid cell level, temporal variability in methane emissions is mainly driven by new well completions, in addition to episodic flaring and liquid unloadings, which are the primary drivers of temporal variability at county and basin levels. While well completion emissions are not large enough in magnitude to drive temporal variability in basin- and county-level emissions, they could stand out at the grid cell level. Temporal variability in hydrocarbons heavier than methane is primarily driven by variability in tank emissions associated with increasing oil production from newly developed wells. Temporal variability in NO_x emissions at the grid level remains dominated by clustered preproduction activities.

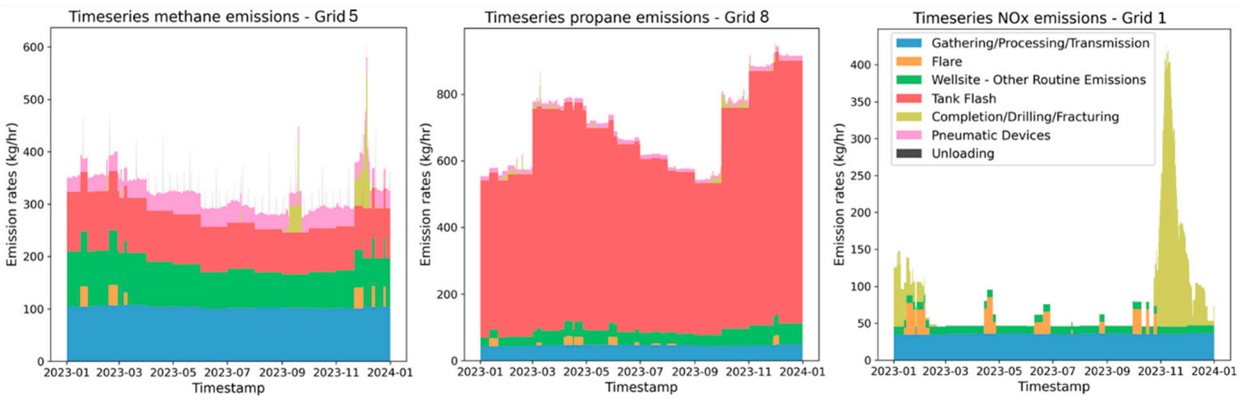

Figure 6. Hourly emission time series for methane (**left**), propane (**middle**), and NO_x (**right**) emissions in the 12-km resolution grids with highest maximum to annual average hourly emission rates ratios in Midland County, Texas in 2023. Grid IDs correspond to those shown in Figure 1.

3.2. Comparison of Temporal and Spatial Variability: Permian vs. Marcellus

The Marcellus inventory for 2023 developed by Chen et al. [14] was updated at the county level using the same simulation methods and sources of data applied in this work. Tank control strategy was updated based on federal regulations as described by Graves et al. [16] to be consistent with the tank controls applied in this work. Emissions in two representative counties, Bradford County in Pennsylvania and Wetzel County in West Virginia that were initially aggregated into 4 km by 4 km grid cells, were re-aggregated into 12 km by 12 km grid cells, to be consistent with the grid resolution in the Permian inventories. A total of 22 grid cells in Bradford County and 6 in Wetzel County were selected for statistical analysis. Most of each grid cell lies within the county boundaries, as shown in the Supplementary Materials. Although the same simulation methods, sources of data, control assumptions, and spatial aggregations were used to facilitate comparison, the comparison may still be limited by differences in data quality between the two basins. Well density and county size may also influence the distribution of spatial and temporal variability.

Table 5 compares maximum to annual average hourly emission rate ratios averaged at the basin, county, and 12 km by 12 km grid cell levels for methane, propane, VOCs and NO_x in the Permian and Marcellus basins in 2023, as an indicator of the level of temporal variability in emissions. Figure 7 shows the distribution of county-level maximum to annual average hourly emission rate ratios in the Permian and Marcellus Basins in 2023, with a wider distribution of ratios indicating greater spatial variability across the counties. Only counties with more than 10 active producing wells were included in analyses. The basin-level and county-level comparisons cover the full study domains, whereas the grid-level comparison is limited to the grid cells within Midland (TX), Bradford (PA), and Wetzel (WV) Counties. The number of grid cells within each selected county may also influence the distribution of temporal and spatial variability. Well density is generally higher in the Permian Basin, which may reduce temporal variability when emissions are aggregated at the same spatial scale relative to the Marcellus, although substantial variability in well distributions exists within both regions.

Table 5. Maximum to annual average hourly emission rate ratios averaged at the basin, county, and 12 km by 12 km grid cell levels in the Permian and Marcellus Basins in 2023.

Species	Basin Level		County-Level Average		Grid-Level Average		
	Permian	Marcellus	Among 55 Counties in Permian	Among 153 Counties in Marcellus	Among 12 Grids in Midland, TX	Among 22 Grids in Bradford, PA	Among 6 Grids in Wetzel, WV
Methane	1.0	1.2	1.3	1.8	1.6	3.8	4.4
Propane	1.0	1.4	1.1	2.4	1.2	3.8	3.0
VOCs	1.0	2.6	1.2	6.4	1.3	4.9	3.0
NO_x	1.1	1.1	1.4	1.3	3.7	1.5	2.5

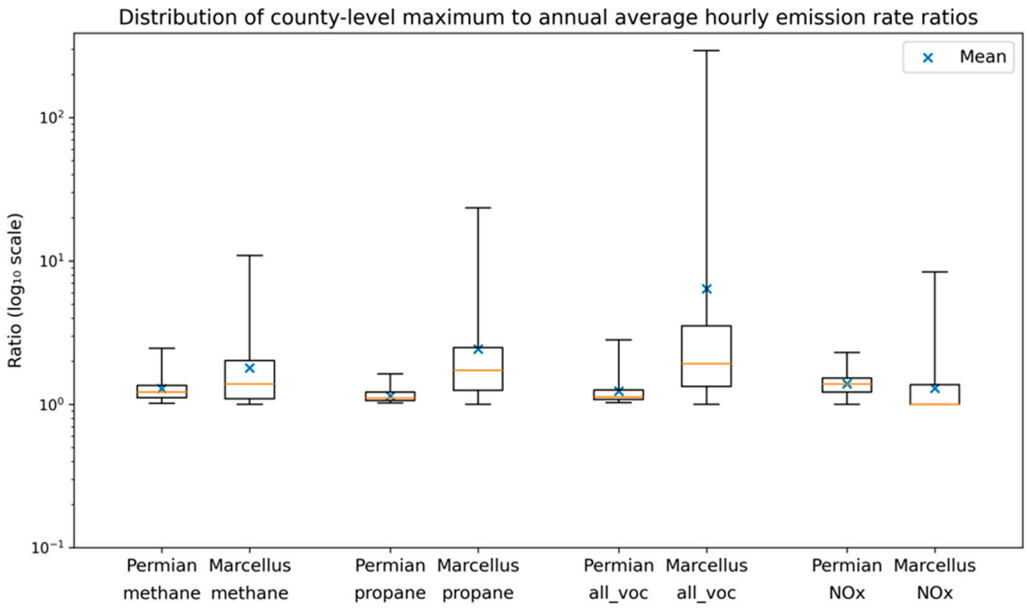

Figure 7. Distribution of county-level maximum to annual average hourly emission rate ratios in the Permian and Marcellus Basins in 2023. The upper and lower whiskers represent the maximum and minimum ratios across counties. The upper and lower bounds of each box represent the 75th and 25th percentiles, respectively. The horizontal line within the box indicates the median, and the cross represents the mean. The *y*-axis is shown on a logarithmic (log_{10}) scale.

In the Permian Basin, the average ratios are lower for hydrocarbon emissions, but higher for NO_x emissions than in the Marcellus at all spatial scales of analysis, indicating lower temporal variability in hydrocarbon emissions but greater variability in NO_x emissions in the Permian. Hydrocarbon emissions in the Permian Basin also exhibit a narrower distribution of ratios, indicating lower spatial variability across counties in the Permian. This difference is primarily due to the lower fraction of episodic sources, such as liquid unloadings, and the higher fraction of emissions from near-continuous sources, such as associated gas venting in the Permian. Temporal variability in hydrocarbon emissions in the Permian, driven primarily by flaring and tank flashing, is substantially smaller than the variability driven by liquid unloadings, which are the primary drivers of temporal variability in the Marcellus. In contrast, NO_x emissions in the Permian show greater temporal variability than in the Marcellus, especially at the grid cell level, due to more frequent pre-production activities associated with the addition of new wells.

3.3. Limitations

The inventories developed in this study have three main limitations.

First, emission estimates depend on the quality and completeness of publicly available activity data, emission factors, and empirical models. Although large measurement datasets were incorporated into the simulations for most well-site sources, this limitation is particularly important for gathering compressor stations and other midstream facilities. Emissions from gathering compressor stations are sensitive to assumptions regarding facility locations and site throughput and could be improved using facility-specific data when available. Emissions from gas processing plants and transmission facilities were assumed to remain constant over time. Because these sources account for a large portion of total emissions, particularly for NO_x, this assumption may reduce the estimated temporal variability. Additional observational data from field measurements and time-resolved operational data should therefore be incorporated when available.

Second, representative hydrocarbon compositions developed primarily from data collected near Midland were applied across the Permian Basin and may not capture regional differences in production characteristics and gas composition. Spatially resolved composition and operating data, particularly separator pressures, which strongly influence speciation estimates, would improve these estimates.

Third, the inventories developed primarily represent emissions from routine operations and do not include unintended emission events due to equipment malfunctions, abnormal operations, or other super emitters, which may contribute substantially to total emissions in the measurement-based inventories. The inventories developed in this work were evaluated against ambient observations in a separate atmospheric modeling study by Graves et al. [16]. Hourly ethane and propane emissions resolved at the 12 km by 12 km grid level were used as inputs to dispersion and chemical transport modeling for representative weeks in 2022, and modeled concentrations were compared with observations from a regional air quality monitor in Midland County, Texas. The modeled time series generally captured the timing of elevated ethane and propane concentrations measured at the regional monitor, indicating that the developed inventory is representative of the temporal variability in routine oil and gas emissions. Differences between predicted and observed concentrations may be attributed to uncertainties in estimated emission magnitudes and contributions from abnormal high-emitting events that are not represented in the inventory.

4. Implications

Spatial and temporal variability in oil and gas emissions, as well as the sources that drive this variability, depend on several factors, including regional production characteristics, the level of spatial aggregation, and emission compositions. Regional production characteristics, such as whether a region is oil production or gas production dominated and the frequency of new well development, have a strong impact on the distribution of operational activities and emission sources, resulting in distinct patterns of spatial and temporal variability in region aggregated emissions. For example, some operations associated primarily with gas wells, such as liquid unloadings, occur much less frequently in the Permian Basin compared to in the Marcellus. Instead, sources related to oil production that have limited contributions in gas-dominated regions, such as associated gas venting, become more important in the Permian. In addition, the Permian Basin, as an oil-dominated region, has more frequent flaring events to combust associated gas from oil wells or excess gas due to limited gas processing infrastructure. As a result, flaring is one of the dominant drivers of temporal variability in methane emissions in the Permian, which is not observed in the Marcellus. Frequent new well development in the Permian also makes well completions an important contributor to temporal variability in methane emissions at certain spatial scales.

The sources driving temporal variability also depend on the level of spatial aggregation and spatial location. Some episodic sources, such as well completions, are not large enough to drive temporal variability at the county or basin level but can substantially influence variability at the 12 km by 12 km grid cell or finer spatial scales, or in subregions with clustered completion events.

The drivers of variability also differ by emission species. Methane variability is primarily influenced by episodic sources with produced gas or well stream compositions that contain high methane fractions. For higher molecular weight hydrocarbons, variability in emissions is increasingly driven by tank flashes which have higher fractions of heavier hydrocarbons in their emission compositions. In contrast, NO_x emissions, that are associated with combustion sources, show completely different patterns of spatial and temporal variability compared with hydrocarbon emissions.

The temporally and spatially resolved NO_x and VOC inventories can support air quality analyses for pollutants such as ozone. Recent measurements and modeling studies have shown that NO_x and VOC emissions from oil and gas operations can strongly influence local ozone production [34–36]. For example, analyses of ozone concentration measurements at a Permian Basin site found that on days when ozone exceeded the national air quality standard, basin-wide column concentrations of NO_2 (a component of NO_x) and HCHO (a proxy for VOC reactivity) across the Permian basin were 8% and 5% higher, respectively, compared with average conditions during the same season. Field measurements showed that alkanes associated with oil and gas operations accounted for 75% of the total OH reactivity of measured VOCs, and NOx was strongly correlated with oil and gas tracers, indicating a strong influence of oil and gas emissions on high-ozone conditions [34]. Compared with conventional inventories that rely on annually and spatially aggregated emissions, the inventories developed in this work provide a higher resolution input for predicting the magnitude, timing, and location of ozone formation and identifying the emission sources and activities driving elevated ozone.

5. Conclusions

Hourly inventories of light alkanes, VOCs, and NO_x were developed for upstream and midstream sources in the Permian Basin for 2022–2024, at the basin level, county level, and 12 km by 12 grid cell level. In 2023, annual average hourly emission rates from routine operations were 129.3 tonnes/h for methane, 421.7 tonnes/h for VOCs, and 30.8 tonnes/h for NO_x. Maximum-to-annual-average hourly emission ratios were calculated at various spatial scales to demonstrate spatial and temporal variability in oil and gas emissions. While VOC and NO_x emissions aggregated at the basin level have maximum hourly rates that are 1.0 and 1.1 times their respective annual averages in the Permian, their maximum hourly rates can be 27 and 14 times their respective annual averages when emissions are aggregated at the 12 km by 12 km grid cell level. Coarsely resolved inventories may therefore miss short-duration, localized emission peaks.

Emission sources that drive spatial and temporal variability also differ by regional production characteristics and emitted species. In 2023, basin-level maximum-to-annual-average hourly emission rate ratios for hydrocarbon emissions were approximately 1 in the Permian, compared with a range of 1–3 in the Marcellus. The lower temporal variability in hydrocarbon emissions in the Permian was due to fewer episodic liquid unloading events that produce highly variable emissions, and greater contributions from near continuous oil production-related sources, such as associated gas venting and tank flashing. In contrast, the basin- and county-level NO_x ratios were comparable between the two regions, but a greater grid-level NO_x variability was observed in Midland County in the Permian than in representative counties in the Marcellus, driven by more frequent, spatially and temporally clustered preproduction activities in Midland.

The inventories and emission variability analyses are limited by uncertainties in activity data and the lack of time-resolved operation information, especially for gathering and midstream facilities. The predicted hydrocarbon composition profiles applied across the basin may also not capture regional differences. Future work should incorporate facility-specific, time-resolved operational data, together with spatially resolved hydrocarbon composition data. Despite these limitations, the inventories provide much finer spatial and temporal resolution than previous large-scale basin level inventories and largely improve the ability to capture localize, short-duration, episodic emission events and to identify the sources driving emission variability. Unintended large emission events may temporarily affect the distributions of spatial and temporal variability in emissions.

The high spatial and temporal resolution inventories can be further combined with chemical transport modeling and air quality and health impact analyses to identify potential hotspots of elevated air pollution. For example, modeling ozone formation based on VOC and NO_x emissions from the spatially and temporally resolved inventories could have the ability to predict both locations and timing of elevated ozone concentrations, as well as the emission sources and oil and gas activities that drive its formation.

Supplementary Materials: The following supporting information can be downloaded at https://www.mdpi.com/article/10.3390/atmos17090870/s1: S1. Production and well counts in the study domain. S2. Distributions of hourly emission rates. S3. Time series of ethane, butane, and VOC emissions. S4. Comparison between well-level simulation and grid-level simulation in Midland County. S5. Sensitivity scenarios. S6. Updates to Marcellus Inventory.

Author Contributions: Conceptualization, D.T.A.; Methodology, Q.C. and S.J.A.; Software, Q.C. and S.J.A.; Validation, Q.C.; Formal analysis, Q.C. and S.J.A.; Investigation, Q.C.; Resources, L.H.R. and D.T.A.; Data curation, Q.C., S.J.A. and S.S.; Writing—original draft, Q.C.; Writing—review & editing, Q.C., S.J.A., S.S., L.H.R. and D.T.A.; Visualization, Q.C.; Supervision, Lea Hildebrandt Ruiz and D.T.A.; Project administration, S.S., L.H.R. and D.T.A.; Funding acquisition, L.H.R. and D.T.A. All authors have read and agreed to the published version of the manuscript.

Funding: Research described in this work was conducted under contract to the Health Effects Institute (HEI), an organization jointly funded by the United States Environmental Protection Agency (EPA) (Contract No. 68HERC19D0010) and certain oil and natural gas companies. Although the research was produced with partial funding by EPA and industry, they have not been subject to their review, and therefore the research does not necessarily reflect the views of the Agency or the oil and natural gas industry, and no official endorsement by the Agency or the industry should be inferred.

Institutional Review Board Statement: Not applicable.

Informed Consent Statement: Not applicable.

Data Availability Statement: The raw data supporting the conclusions of this article will be made available by the authors on request.

Conflicts of Interest: The authors declare the following competing financial interest(s): D.T.A. and L.H.R have served on the Environmental Protection Agency's Science Advisory Board; in this role, they were Special Governmental Employees. D.T.A.'s research is currently supported by the National Science Foundation, the Department of Energy, the Texas Commission on Environmental Quality, Chevron, ExxonMobil, and the Environmental Defense Fund. He has also worked on air quality projects that have been supported by oil and gas producers and the Environmental Defense Fund. D.T.A. has worked as a consultant for multiple companies, including British Petroleum, Cheniere, Eastern Research Group, KeyLogic, and SLR International. L.H.R.'s research is supported by the Texas Commission on Environmental Quality, the Health Effects Institute, the Welch Foundation and ExxonMobil.

References

1. U.S. Energy Information Administration (EIA). *U.S. Crude Oil Production Rose by 2% in 2024*; U.S. Energy Information Administration (EIA): Washington, DC, USA, 2025. Available online: https://www.eia.gov/todayinenergy/detail.php?id=65024 (accessed on 8 March 2026).
2. U.S. Energy Information Administration (EIA). *U.S. Natural Gas Production Remained Flat in 2024*; U.S. Energy Information Administration (EIA): Washington, DC, USA, 2025. Available online: https://www.eia.gov/todayinenergy/detail.php?id=65025 (accessed on 8 March 2026).
3. Modi, M.; Kimura, Y.; Hildebrandt Ruiz, L.; Allen, D.T. Fine Scale Spatial and Temporal Allocation of NOx Emissions from Unconventional Oil and Gas Development Can Result in Increased Predicted Regional Ozone Formation. *ACS ES T Air* **2025**, *2*, 130–140. [CrossRef] [PubMed]
4. Cusworth, D.H.; Duren, R.M.; Thorpe, A.K.; Olson-Duvall, W.; Heckler, J.; Chapman, J.W.; Eastwood, M.L.; Helmlinger, M.C.; Green, R.O.; Asner, G.P.; et al. Intermittency of Large Methane Emitters in the Permian Basin. *Environ. Sci. Technol. Lett.* **2021**, *8*, 567–573. [CrossRef]
5. Chen, Y.; Sherwin, E.D.; Berman, E.S.F.; Jones, B.B.; Gordon, M.P.; Wetherley, E.B.; Kort, E.A.; Brandt, A.R. Quantifying Regional Methane Emissions in the New Mexico Permian Basin with a Comprehensive Aerial Survey. *Environ. Sci. Technol.* **2022**, *56*, 4317–4323. [CrossRef] [PubMed]
6. Rutherford, J.S.; Sherwin, E.D.; Ravikumar, A.P.; Heath, G.A.; Englander, J.; Cooley, D.; Lyon, D.; Omara, M.; Langfitt, Q.; Brandt, A.R. Closing the Methane Gap in U.S. Oil and Natural Gas Production Emissions Inventories. *Nat. Commun.* **2021**, *12*, 4715. [CrossRef] [PubMed]
7. Zhang, Y.; Gautam, R.; Pandey, S.; Omara, M.; Maasakkers, J.D.; Sadavarte, P.; Lyon, D.; Nesser, H.; Sulprizio, M.P.; Jacob, D.J. Quantifying Methane Emissions from the Largest Oil-Producing Basin in the United States from Space. *Sci. Adv.* **2020**, *6*, eaaz5120. [CrossRef] [PubMed]
8. Vaughn, T.L.; Bell, C.S.; Pickering, C.K.; Schwietzke, S.; Heath, G.A.; Pétron, G.; Zimmerle, D.J.; Schnell, R.C.; Nummedal, D. Temporal Variability Largely Explains Top-Down/Bottom-Up Difference in Methane Emission Estimates from a Natural Gas Production Region. *Proc. Natl. Acad. Sci. USA* **2018**, *115*, 11712–11717. [CrossRef] [PubMed]
9. U.S. Environmental Protection Agency. *Inventory of U.S. Greenhouse Gas Emissions and Sinks: 1990–2022*; EPA: Washington, DC, USA, 2024. Available online: https://www.epa.gov/ghgemissions/inventory-us-greenhouse-gas-emissions-and-sinks-1990-2022 (accessed on 9 July 2025).
10. U.S. Environmental Protection Agency. *EPA Facility Level GHG Emissions Data*; EPA: Washington, DC, USA, 2024. Available online: https://ghgdata.epa.gov/ghgp/main.do (accessed on 9 July 2025).
11. U.S. Environmental Protection Agency. National Emissions Inventory (NEI). Available online: https://www.epa.gov/air-emissions-inventories/national-emissions-inventory-nei (accessed on 12 August 2025).
12. Texas Commission on Environmental Quality. Point Source Emissions Inventory. Available online: https://www.tceq.texas.gov/airquality/point-source-ei (accessed on 12 August 2025).
13. Omara, M.; Gautam, R.; O'Brien, M.A.; Himmelberger, A.; Franco, A.; Meisenhelder, K.; Hauser, G.; Lyon, D.R.; Chulakadaba, A.; Miller, C.C.; et al. Developing a Spatially Explicit Global Oil and Gas Infrastructure Database for Characterizing Methane Emission Sources at High Resolution. *Earth Syst. Sci. Data* **2023**, *15*, 3761–3790. [CrossRef]
14. Chen, Q.; Raksi, N.; Niewenhous, L.; Almasalha, S.J.; Graves, J.D.; Brown, V.; Stokes, S.; Allen, D.T.; Hildebrandt Ruiz, L. Spatial and Temporal Variability in Atmospheric Emissions from Oil and Gas Sector Sources in the Marcellus Production Region. *Atmosphere* **2025**, *16*, 1048. [CrossRef]
15. Enverus. Available online: https://prism.enverus.com/prism/home (accessed on 3 November 2024).
16. Graves, J.D.; Chen, Z.; Chen, Q.; Kimura, Y.; Navarro Brown, V.; Allen, D.T. Hybrid Dispersion and Chemical Transport Modeling Frameworks for Characterizing Sources of Ambient Hydrocarbons in the Permian Basin. *Atmos. Environ.* **2026**, *383*, 122300. [CrossRef]

17. Esri. World Imagery. Available online: https://services.arcgisonline.com/ArcGIS/rest/services/World_Imagery/MapServer (accessed on 10 July 2025).
18. Earth Observation Group. Global Gas Flaring Observed from Space. Available online: https://eogdata.mines.edu/products/vnf/global_gas_flare.html (accessed on 8 March 2026).
19. Elvidge, C.; Zhizhin, M.; Baugh, K.; Hsu, F.-C.; Ghosh, T. Methods for Global Survey of Natural Gas Flaring from Visible Infrared Imaging Radiometer Suite Data. *Energies* **2015**, *9*, 14. [CrossRef]
20. Elvidge, C.; Zhizhin, M.; Hsu, F.-C.; Baugh, K. VIIRS Nightfire: Satellite Pyrometry at Night. *Remote Sens.* **2013**, *5*, 4423–4449. [CrossRef]
21. Zhizhin, M.; Matveev, A.; Ghosh, T.; Hsu, F.-C.; Howells, M.; Elvidge, C. Measuring Gas Flaring in Russia with Multispectral VIIRS Nightfire. *Remote Sens.* **2021**, *13*, 3078. [CrossRef]
22. Earth Observation Group. VIIRS Nightfire. Available online: https://eogdata.mines.edu/products/vnf/ (accessed on 8 March 2026).
23. Cardoso-Saldaña, F.J.; Pierce, K.; Chen, Q.; Kimura, Y.; Allen, D.T. A Searchable Database for Prediction of Emission Compositions from Upstream Oil and Gas Sources. *Environ. Sci. Technol.* **2021**, *55*, 3210–3218. [CrossRef] [PubMed]
24. Allen, D.T.; Cardoso-Saldaña, F.J.; Kimura, Y. Variability in Spatially and Temporally Resolved Emissions and Hydrocarbon Source Fingerprints for Oil and Gas Sources in Shale Gas Production Regions. *Environ. Sci. Technol.* **2017**, *51*, 12016–12026. [CrossRef] [PubMed]
25. U.S. Environmental Protection Agency. 2020 Nonpoint Oil and Gas Emissions Estimation Tool V1.3. Available online: https://gaftp.epa.gov/Air/nei/2020/doc/supporting_data/nonpoint/oilgas/OIL_GAS_TOOL_v1.3/ (accessed on 9 July 2025).
26. U.S. Environmental Protection Agency. AP-42: Compilation of Air Emissions Factors from Stationary Sources. Available online: https://www.epa.gov/air-emissions-factors-and-quantification/ap-42-compilation-air-emissions-factors-stationary-sources (accessed on 9 July 2025).
27. Allen, D.T.; Cardoso-Saldaña, F.J.; Kimura, Y.; Chen, Q.; Xiang, Z.; Zimmerle, D.; Bell, C.; Lute, C.; Duggan, J.; Harrison, M. A Methane Emission Estimation Tool (MEET) for Predictions of Emissions from Upstream Oil and Gas Well Sites with Fine Scale Temporal and Spatial Resolution: Model Structure and Applications. *Sci. Total Environ.* **2022**, *829*, 154277. [CrossRef] [PubMed]
28. Vaughn, T.L.; Luck, B.; Williams, L.; Marchese, A.J.; Zimmerle, D. Methane Exhaust Measurements at Gathering Compressor Stations in the United States. *Environ. Sci. Technol.* **2021**, *55*, 1190–1196. [CrossRef] [PubMed]
29. Zimmerle, D.; Vaughn, T.; Luck, B.; Lauderdale, T.; Keen, K.; Harrison, M.; Marchese, A.; Williams, L.; Allen, D. Methane Emissions from Gathering Compressor Stations in the U.S. *Environ. Sci. Technol.* **2020**, *54*, 7552–7561. [CrossRef] [PubMed]
30. Allen, D.T.; Sullivan, D.W.; Zavala-Araiza, D.; Pacsi, A.P.; Harrison, M.; Keen, K.; Fraser, M.P.; Daniel Hill, A.; Lamb, B.K.; Sawyer, R.F.; et al. Methane Emissions from Process Equipment at Natural Gas Production Sites in the United States: Liquid Unloadings. *Environ. Sci. Technol.* **2015**, *49*, 641–648. [CrossRef] [PubMed]
31. Allen, D.T.; Pacsi, A.P.; Sullivan, D.W.; Zavala-Araiza, D.; Harrison, M.; Keen, K.; Fraser, M.P.; Daniel Hill, A.; Sawyer, R.F.; Seinfeld, J.H. Methane Emissions from Process Equipment at Natural Gas Production Sites in the United States: Pneumatic Controllers. *Environ. Sci. Technol.* **2015**, *49*, 633–640. [CrossRef] [PubMed]
32. Allen, D.T.; Torres, V.M.; Thomas, J.; Sullivan, D.W.; Harrison, M.; Hendler, A.; Herndon, S.C.; Kolb, C.E.; Fraser, M.P.; Hill, A.D.; et al. Measurements of Methane Emissions at Natural Gas Production Sites in the United States. *Proc. Natl. Acad. Sci. USA* **2013**, *110*, 17768–17773. [CrossRef] [PubMed]
33. Environmental Protection Agency. *40 CFR Part 60 Subpart OOOOa—Standards of Performance for Crude Oil and Natural Gas Facilities for Which Construction, Modification or Reconstruction Commenced After September 18, 2015 and On or Before December 6, 2022*; Environmental Protection Agency: Washington, DC, USA, 2016. Available online: https://www.ecfr.gov/current/title-40/chapter-I/subchapter-C/part-60/subpart-OOOOa (accessed on 11 March 2026).
34. Marsavin, A.; Pan, D.; Zhou, Y.; Pollack, I.B.; Sullivan, A.P.; Sive, B.C.; Prenni, A.J.; Schichtel, B.; Fischer, E.V.; Collett, J.L. Examining Ozone Production in the Permian Oil and Gas Basin Using Carlsbad Caverns National Park Measurements and Satellite Data. *ACS ES T Air* **2026**. [CrossRef]
35. Pan, D.; Pollack, I.B.; Sive, B.C.; Marsavin, A.; Naimie, L.E.; Benedict, K.B.; Zhou, Y.; Sullivan, A.P.; Prenni, A.J.; Cope, E.J.; et al. Source Characterization of Volatile Organic Compounds at Carlsbad Caverns National Park. *J. Air Waste Manag. Assoc.* **2023**, *73*, 914–929. [CrossRef] [PubMed]
36. Marsavin, A.; Pan, D.; Pollack, I.B.; Zhou, Y.; Sullivan, A.P.; Naimie, L.E.; Benedict, K.B.; Juncosa Calahorrano, J.F.; Fischer, E.V.; Prenni, A.J.; et al. Summertime Ozone Production at Carlsbad Caverns National Park, New Mexico: Influence of Oil and Natural Gas Development. *J. Geophys. Res. Atmos.* **2024**, *129*, e2024JD040877. [CrossRef]